Title
Lifespan Changes of the Human Insula in Major Depression

Permalink
https://escholarship.org/uc/item/2tj4g0w0

Author
Myoraku, Alison

Publication Date
2019

Peer reviewed|Thesis/dissertation

Lifespan Changes of the Human Insula in Major Depression

by
Alison Myoraku

THESIS
Submitted in partial satisfaction of the requirements for degree of
MASTER OF SCIENCE

in

Biomedical Imaging

in the

GRADUATE DIVISION
of the
UNIVERSITY OF CALIFORNIA, SAN FRANCISCO

Approved:

DocuSigned by:

Duygu Tosun-Turgut
A2C3822F2671486...

Duygu Tosun-Turgut
Chair

DocuSigned by:

Irina Strigo

Irina Strigo

DocuSigned by:

Valentina Pedoia

Valentina Pedoia

DocuSigned by:

Ashish Raj
13BDA73A066E4E0...

Ashish Raj

Committee Members

Copyright 2019

by

Alison Myoraku

Acknowledgements

First and foremost, I would like to thank Dr. Duygu Tosun-Turgut for serving as the chair of my committee and offering such unwavering support and guidance throughout this process. I would also like to thank Dr. Irina Strigo for helping me to obtain the necessary data for this project and for sharing her expertise on insular function in major depression. Lastly, I would like to acknowledge the shared expertise and valuable feedback provided by my other two committee members, Dr. Valentina Pedoia, and Dr. Ashish Raj.

<p style="text-align: center">Lifespan Changes of the Human Insula in Major Depression</p>

<p style="text-align: center">Alison Myoraku</p>

Abstract

Using cross-sectional structural magnetic resonance imaging (MRI) data from six cohorts originating from three sites, this study investigated the cortical morphometric trajectories of six insular subregions of individuals with major depressive disorder (MDD) compared to healthy individuals across the lifespan to better understand the neurodevelopmental and neurodegeneration aspects of MDD. The insula is a centrally located region of the brain responsible for emotional regulation and awareness and has been implicated in many psychiatric disorders including MDD. Participants across all sites included in this study totaled 203 individuals with current MDD (F=137, M=66) and 215 healthy controls (F=110, M=105). T1-weighted magnetic resonance (MR) images from each cohort were registered and segmented using Advanced Normalization Tools (ANTs) and a 3D probabilistic atlas of the human brain, including the following insular regions: posterior long gyrus, anterior long gyrus, anterior short gyrus, middle short gyrus, posterior short gyrus, and anterior inferior cortex. In addition, we examined the amygdala, anterior cingulate gyrus, lateral occipital cortex, cuneus, subgenual cortex, and lateral orbitofrontal cortex. The outputs were then standardized and harmonized to adjust site effects in morphometric measurements while preserving biological variation due to age, sex, relative intracranial volume, and diagnosis. We hypothesized that the relationships among morphometric measures and age are dynamic across the lifespan and influenced by MDD. For each region of interest considered in this study, linear, quadratic, and cubic models were tested to model morphometry and age association first within each group separately and then tested for group-age interaction. Our statistical analyses indicate that the volumes of all insular subregions in the left hemisphere, as well as the right anterior short gyrus, middle short gyrus and anterior long gyrus, exhibited a significant age-associated difference between the control and MDD groups. Furthermore, the group-age interaction revealed that these deviations were particularly significant for 60-79 years of age, indicating co-morbidity of depression with neurodegeneration. Most non-insular

regions showed significant differences between groups, but association with age was less robust. Results

for the surface area analysis were less conclusive. Further analysis of other metrics related to

neurodevelopment (i.e. cortical thickness) will better inform this facet of the disease.

Table of Contents

List of Figures

List of Tables

Chapter 1: Introduction

Major depressive disorder (MDD) is a debilitating disorder that affects approximately 300 million people worldwide.[1] Despite its prevalence, numerous questions about depression remain unanswered, namely whether it is co-morbid with neurodegeneration or a consequence of inheritance and neurodevelopment. Furthermore, many patients tend to receive the same types of treatment regardless of the etiology of their symptoms. Characterizing the trajectory of neurodevelopment and neurodegeneration in patients with MDD could provide an objective, measurable biomarker of the disease, something that is currently lacking for many psychiatric disorders and could contribute to the development of personalized treatments.

The insula, also known as "the island of Reil," is located deep within the lateral sulcus. It is divided into two main regions - the larger agranular anterior insula and the smaller granular posterior insula - which both contain further subdivisions. The insula plays a pivotal role in our concept of self-awareness, including the awareness of our bodies and emotions, and how they interact to create our perception of the present moment. It is also involved in various emotion processes and psychopathological symptoms including depression, anxiety, pain, and many others.[2] Furthermore, it serves as a center for interoceptive awareness, or the "sense of the physiological condition of the body."[2] Functionality of the insula (especially the anterior region) is also implicated in adaptive emotional responding and emotional intelligence.[3]

Current literature implicates the insula's role in depression from both functional and morphological standpoints and emphasizes the reproducibility of these findings. One meta-analysis that included 73 studies (1736 depressed patients and 2365 healthy controls) found decreased volume in the left insula in the patient group compared to controls.[4] Another meta-analysis focused on essential brain structural alterations in MDD also found decreased volume in the left insula and speculated that these volumetric deviations in MDD patients may serve as the foundation for the functional difference also found within this region.[5]

For the purposes of this study, we investigated morphological changes in the following six subdivisions in each hemisphere of the insula as outlined by the template created by Faillenot et al: posterior insula (posterior long gyrus and anterior long gyrus), anterior insula (anterior short gyrus, middle short gyrus, posterior short gyrus), and the anterior inferior cortex.[6] Due to its centrality, the insula shares connections with multiple cortical and subcortical regions that can vary by hemisphere and subregion. For example, the insula is fully connected to the thalamus, putamen, and caudate, but anterior insular connections with the thalamus are implicated in autonomic function and emotional processing, while posterior insular connections to the same region are implicated in auditory and somatosensory processing.[7] Posterior regions of the insula are also connected to the hippocampus, globus pallidus, and amygdala while the anterior region connects to the nucleus accumbens. Ghaziri et al implemented high angular resolution diffusion imaging (HARDI) to track connections between the insula and the frontal, parietal, occipital, and temporal lobe and found that the right insula appears more fully connected than the left.[7]

The insula's centrality in the brain accedes its high metabolic demand, predisposing it to dysfunction in disease. It is also one of the first regions to develop and fold during gestation.[8] The functional profile and vulnerability to degeneration varies across the insular sub-regions, making it an interesting target for trajectory analysis.[9] In a cohort of healthy participants, investigators found that anterior insula volume exhibits a linear developmental trajectory, while posterior insula volume fits a more complex quadratic or cubic trajectory within the first three decades of life.[10] Our project extended the trajectory into middle-aged and late-life cohorts to examine how the morphology of the insula changes over time in individuals with and without psychopathological symptoms, particularly MDD.

The current study investigated the morphometric trajectories of various regions of the insula over the lifespan of unmedicated patients with current MDD compared to healthy participants without history of MDD. Using structural T1-weighted (T1w) magnetic resonance (MR) images, parcellation of the insula and examination of geometry and volume of each region allowed for modeling of

neurodevelopment and neurodegeneration in its multiple regions. Investigation of the geometry of insular regions is of particular interest, as most current literature focuses on volume analyses. A similar analysis was conducted on multiple other brain regions implicated in depression (amygdala, subgenual cortex, lateral orbitofrontal cortex, and anterior cingulate gyrus) to ensure deviations from normal lifespan trajectories observed in the insula are unique to that brain region, as opposed to a global effect. These dynamic profiles will provide an understanding of the deviation between the trajectories of the healthy controls and MDD patients in each subregion, with focus on the point and duration of deviation throughout the lifespan.

Chapter 2: Materials and Methods

2.1 Dataset descriptions

Access to cohorts spanning over a wide age spectrum is crucial in the assessment of lifespan trajectories of neurodevelopment and neurodegeneration jointly. This collaborative investigation to assess lifespan trajectory of insular morphology leveraged six cohorts of MDD and matched healthy subjects recruited at three research sites. Specifically, T1w MR scans from three sites were aggregated to study structural changes of the insula across the lifespan of subjects with and without MDD.

Adolescent cohort: Stanford University provided brain images of 71 MDD subjects (F=53, M=18) and 41 images of healthy control subjects (F=17, M=24), with age ranges of 13–18 years and 13–17 years, respectively. Thirty-one of the MDD cases and nine of the healthy control cases were acquired on a GE 3T scanner with the following imaging parameters: TR = 8.2 ms, TE = 3.2 ms, TI = 600 ms, flip angle = 12°, 156 axial slices, FOV = 25.6 cm, 256 x 256 mm matrix, 1 x 1 x 1 mm^3 voxels. The remaining images were acquired on a GE 3T scanner with the following acquisition parameters: TR = 6.24 ms, TE = 2.34 ms, TI = 450 ms, flip angle = 12°, 186 sagittal slices, FOV = 23 cm, 256 x 256 mm matrix, 0.8984 x 0.8984 x 0.9 mm^3 voxels. For the purposes of harmonization, this cohort was split into two groups which will be referred to as Adolescent 1 and Adolescent 2.

Young Adult cohort: The University of California, San Diego contributed data from two separate studies, but with overlapping ages. All of the images were acquired on the same GE 3T scanner, but each study used different imaging parameters. The first cohort consists of 52 images of MDD subjects (F=30, M=22) and 55 images of healthy controls (F=21, M=34), with age ranges of 18-49 and 18-38 years respectively. These images were acquired with a fast-spoiled gradient-recalled echo sequence with the following parameters: TR = 8 ms, TE = 3 ms, TI = 450 ms, flip angle = 12°, FOV = 25 cm, 172 sagittal slices, 256 x 256 mm matrix, 1 x 0.97 x 0.97 mm^3 voxels.

The second cohort consists of 45 images of healthy controls (F= 21, M =24), with an age range of 30-63 years. These images were acquired on three scanner models across seven facilities (Phillips Achieva, GE MR750, and Siemens TimTrio). A chi-square analysis was conducted to confirm that there were no statistically significant differences in the distribution of groups by scanner (χ^2= 7.38, $p > .1$). The acquisition parameters are as follows: TR_{GE}=9.16, $TR_{Phillips}$=7.64, 7.67, $TR_{Siemens}$=2530; TE_{GE}=3.71, 3.68, $TE_{Phillips}$=3.56, 3.53, $TE_{Siemens}$=3.32; 256 x 256 matrix, flip angle$_{GE}$=10 flip angle$_{Phillips}$=7, flip angle$_{Siemens}$=7; field of view=256mm; 176 sagittal slices, 1mm slice thickness, Phillips= 3D Turbo Field Echo, GE = Inversion recovery prepared fast spoiled gradient echo, Siemens = magnetization-prepared rapid gradient echo sequence).

Middle-aged cohort: The University of California, San Francisco contributed 29 images of MDD subjects (F=16, M=13) and eight images of healthy controls (F=5, M=3), with age ranges of 22-55 and 24-52 respectively. Images were acquired with an MPRAGE sequence on a Siemens Skyra 3T scanner with the following parameters: TR=2300 ms, TE= 2.98 ms, TI = 1000 ms, flip angle = 9°, 256 x 256 mm matrix, 192 slices, 1 x 1 x1 mm^3, FOV = 25.6 cm.

Geriatric cohort: The University of California, San Francisco contributed 51 images of MDD subjects (F=38, M=13) and 66 images of healthy controls (F=46, M=20), with age ranges of 65-85 and 56-85 respectively. Images for healthy controls were acquired on a Siemens 3T Skyra scanner with the following parameters: TR=2300 ms, TE=2.98, TI =900 ms, flip angle = 9°, 256 x 256 mm matrix, 176

sagittal slices, 1 x 1 x 1 mm^3, FOV = 25.6 cm. The healthy control cases were taken from the ADNI2 data

set, which pools data across multiple sites. Although scanners may be different at each site, the ADNI

protocol ensures that the acquisition parameters are tailored to each site to produce the same image

quality across the population.

Table 2.1. Dataset descriptions for MDD data. For the last column, the average age is presented with the standard deviation in parentheses and the interval in brackets.

Dataset	# of participants	Gender	Age in years
Adolescent 1	31	F=23, M=8	16.21 (1.43) [13-18]
Adolescent 2	40	F=30, M=10	16.14 (1.14) [13-18]
Young Adult 1	52	F=30, M=22	26.56 (7.29) [18-49]
Young Adult 2*			
Middle-Age	29	F=16, M=13	36.68 (10.80) [22-55]
Geriatric	51	F=38, M=13	70.24 (4.75) [65-85]
Total	203	F= 137, M=66	

*data not available at time of analysis

Table 2.2 Dataset descriptions for healthy control data. For the last column, the average age is presented with the standard deviation in parentheses and the interval in brackets.

Dataset	# of participants	Gender	Age in years
Adolescent 1	9	F= 4, M=5	15.54 (0.93) [13-16]
Adolescent 2	32	F=13, M= 19	15.48 (0.85) [14-17]
Young Adult 1	55	F=21, M=34	25.24 (5.21) [18-38]
Young Adult 2	45	F=21, M=24	44.20 (10.09) [30-63]
Middle-Age	8	F=5, M=3	35.89 (8.45) [24-52]
Geriatric	66	F=46, M=20	71.95 (6.71) [56-85]
Total	215	F =110, M=105	

2.2 Clinical outcome measures

All depression subjects were diagnosed by a psychiatrist and met DSM-IV criteria for MDD.

Symptom severity was assessed with multiple scales across the cohorts.

Adolescent cohort: This cohort used both the Children's Depression Rating Scale (CDRS) and the

Patient Health Questionnaire-9 (PHQ-9) for the MDD group. All except one participant had a CDRS

score, with raw scores averaging 53.90 (11.87), while 74 of the 76 participants reported PHQ-9 scores

with an average of 14.77 (4.94). The 42 controls were assessed with either the CDRS and PHQ-9 (9) or

the Children's Depression Inventory (CDI) (33) with average scores of 17.40 (1.33), 1.89 (2.26), and 1.73 (1.47) respectively.

Young Adult cohort: Participants in the adult cohort reported depression severity with the Beck Depression Inventory-II (BDI-II), with average scores of 25.06 (10.10) and 1.56 (2.66) for the MDD and healthy controls respectively.

Middle-aged cohort: Depression severity was reported with the Quick Inventory of Depressive Symptomatology (QIDS) for both the healthy controls and MDD patients, with average scores of 2.625 (1.69) and 14.77 (3.84) respectively.

Geriatric cohort: Lastly, the control group of the geriatric cohort was assessed with the Geriatric Depression Scale (GDS) with an average score of 1.04 (1.21). The MDD group was assessed with both the HAM-D 17 and 24, with the following average scores of 18.52 (3.40) and 25.31 (4.41) respectively.

2.3 Quality assurance

Images were visualized with MRIcron to check for outstanding artifacts and the overall quality of the acquisition. Two control images from the adolescent cohort (one from each subset) were removed due to poor quality. Another visual check was performed following the ANTs registration to ensure adequate registration and segmentation. The geriatric cohort went through an additional preprocessing for intensity inhomogeneity correction, using the N4BiasFieldCorrection script in ANTs.

2.4 Registration and Segmentation

The Advanced Normalization Tools script,[11] or ANTs, allows for transformation of labeled data from MNI template space to individual space via affine and SyN registration. After the two images are properly aligned, ANTs uses binary masks of the regions of interest to segment the subject image and generate numeric results, including volume, surface area, eccentricity, elongation, orientation, centroid, axes length, and bounding box. The script contains 95 regions of interest and
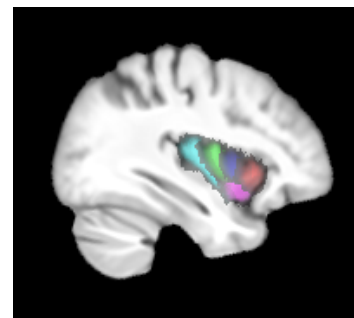

Figure 2.1 Segmentation of the 6 subregions of the insula in the right hemisphere

corresponding binary masks, but for the purposes of this project, only the following regions were considered: insula (posterior long gyrus (PLG), anterior short gyrus (ASG), middle short gyrus (MSG), posterior short gyrus (PSG), anterior inferior cortex (AIC), and the anterior long gyrus (ALG) (see Figure 2.1), the anterior cingulate gyrus, the amygdala, the cuneus, the subgenual cingulate cortex, and the lateral orbitofrontal cortex. The cuneus is not specific to depression and served as a control region, while the amygdala, subgenual cingulate cortex, and lateral orbitofronal cortex served as a comparison for the reasonability of our findings in the insula.

2.5 Harmonization

The challenges of data harmonization are daunting, particularly when imaging biomarker data are combined across multiple studies to achieve optimum power for testing the hypotheses. In order to adjust for site effects on morphometric measurements due to data acquisition on multiple scanners with different image acquisition parameters, we employed a statistical harmonization approach, i.e., ComBat, which models site-specific scaling factors and uses an Empirical Bayes approach that can be scaled to any quantity of data. Originally created to remove batch effects in genomic analysis, this method has been adapted to allow for additive and multiplicative changes to the imaging feature measurements.[12,13,14] It assumes that these measurements can be described by a linear model comprising biological variables of interest and site effects, as well as an error term resulting from other site-specific factors. The following equation outlines the process for calculating the harmonized values,

$$y_{ijv}^{ComBat} = \frac{y_{ijv} - \hat{\alpha}_v - X_{ij}\hat{\beta}_v - \gamma_{iv}^*}{\delta_{iv}^*} + \hat{\alpha}_v + X_{ij}\hat{\beta}_v$$

where $\hat{\alpha}_v$ is the estimated average volume for the reference site, γ_{iv}^* is the additive site effect of the j-th site volume, X is the design matrix for covariates of interest, β_v is the vector of coefficients associated with X for feature v, and δ_{iv}^* is the multiplicative site effect of the j-th site volume.

To ensure that the harmonization process does not eliminate measurement variation due to the biological variables of interest, we include age, sex, diagnosis, and relative intracranial volume (ICV) as covariates. To accommodate the non-linearity of the data over the lifespan, we also included age^2 and

age[3] as covariates. The relative ICV-to-template size was determined by calculating the determinant of the affine registration matrix from the ANTs registration. To account for differences between the resolution of each acquisition and the voxel dimensions of the imaging space, each cohort was scaled to mm^3 unit by a factor of: Adolescent 1: 1.0, Adolescent 2: 0.7264, Young Adult: 0.9409, Middle-aged: 1.0, Geriatric controls: 1.0, and Geriatric MDD: 1.2. The harmonization was run separately for left and right hemisphere regions to account for potential geometric distortion due to B_0 and B_1 inhomogeneities of the magnetization during image acquisition that could lead to differences in signal between the two hemispheres. All ComBat harmonization was run in MATLAB (The MathWorks, Inc., Natick, Massachusetts, United States).

Once harmonization was complete, we conducted a multivariate linear regression of pre- and post-harmonization volumes in terms of age, sex, diagnosis, and site to confirm that the process had successfully eliminated significant differences between sites. In all cases except for the left and right anterior cingulate gyrus, the co-efficient for site was no longer significant after harmonization.

2.6 Statistical analyses

Following registration, segmentation, and harmonization of the images, the processed volumetric and geometric data were adjusted for relative ICV by dividing the values by the determinant of the affine registration matrix (scaling factor). Thirteen outliers (defined as a Z-score outside of the -3 to 3 range) were removed prior to modeling, resulting in the total numbers reflected in Tables 2.1 and 2.2. We then conducted a univariate analysis of each variable (disease status (group), age, and sex) to assess significance before moving on to investigations of interactions between disease status and age. Age was converted into a categorical variable by decade and analyzed with the 30s as the reference group. If disease status was not significant for a subregion, that subregion was not considered for the next step of modeling trajectories.

2.7 Modeling of lifespan trajectories

The data was then plotted and fit to various models (below) to characterize the nature of the trajectory over the lifespan within controls and MDD groups as an interaction between age and disease status (healthy or MDD).[15,16]

Linear model: $Vol = \beta_0 + \beta_1 Age + \varepsilon$

Quadratic model: $Vol = \beta_0 + \beta_1 Age + \beta_2 Age^2 + \varepsilon$

Cubic model: $Vol = \beta_0 + \beta_1 Age + \beta_2 Age^2 + \beta_3 Age^3 + \varepsilon$

For each group, the model was only kept if the F statistic from an ANOVA between the model and the constant model is significant ($p < 0.05$) and if all coefficients are significant with a t-statistic ($p < 0.05$). Once all significant models were established, we used Bayesian information criterion (BIC) to pick the model that best balances bias and variance, allowing us to select the model that explains the most data with the fewest parameters. This process was repeated bilaterally for each brain region under investigation in the study, for both volumetric and geometric data. All statistics were run in R.[17]

Chapter 3: Results

3.1 Harmonization

Harmonization works best when the data in each group exhibit some degree of overlap in the biological variability of interest, i.e., age. Figure 3.1 displays each step of processing the volumes underwent prior to statistical analysis. For all of the subregions in the geriatric cohort, the additive site effect was negative, implying an over-estimation of volumes at this site. With the exception of the anterior inferior cortex in the Young Adult 2 (YA2) and middle-aged cohort, all other additive site effects were positive. The multiplicative site effects, i.e. variance in measurements, were variable across cohorts, reflecting different levels of biological heterogeneity expected at different age groups.
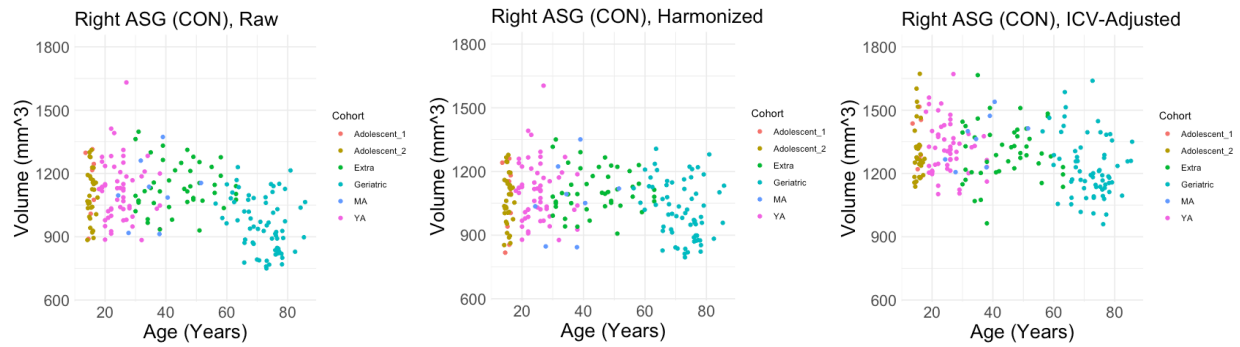
Figure 3.1 Right anterior short gyrus volumes (ASG, left to right: raw volumes from ANTs; harmonized volumes after ComBat; ICV-adjusted volumes calculated by dividing the harmonized volumes by the relative ICV for each case).

3.2 Univariate Analysis

3.2.1. Volume

The univariate analysis conducted on all subregions of both hemispheres revealed the relative contributions of each variable to the predicted volume of the model. In all cases where the coefficient of the group variable was significant, having MDD was associated with lower predicted volume by 11.69 to 892.50 mm^3 depending on the subregion (Table 3.1). All regions for which the coefficient for group was not significant in the univariate analysis (left anterior cingulate gyrus, right PLG, right PSG and right AIC) were not considered in the modeling stage of the analysis.

For age as a categorical variable with 30-39 years of age as the reference group, all insular subregions in both hemispheres exhibited significance in at least one age category except for the left PSG (see table in Appendix I). For the regions of interest outside of the insula, all except for the left subgenual cortex and right cuneus were significant in at least one age category. For the univariate analysis of sex, the coefficient was significant for the following regions: left PLG, left PSG, left and right AIC, left and right amygdala, and left and right lateral orbitofrontal cortex. In all cases except the amygdala, being male was associated with lower volume (anywhere from 26.38 to 571.3 mm^3 - see table in Appendix II).

3.2.2 Surface Area

In contrast to the observations about volume, the univariate analysis of surface area revealed only a few subregions (left and right AIC, right PLG, and right PSG) with significant differences between the two groups (Table 3.2). For these regions, having major depression was associated with an increase in surface area. For age with 30-39 years of age as the reference group, all regions for both hemispheres (with the exception of the anterior cingulate gyrus) were significant for ages 10-19. Almost all regions in the left hemisphere and many in the right were significant for ages 60-69 (see Appendix III). All regions in both hemispheres exhibited very significant differences in surface area based on sex (see Appendix IV).

Table 3.1 Univariate analysis by group to assess difference between volumes of regions of interest in healthy controls and patients with MDD.

Left	Co-efficient	P-value	Right	Co-efficient	P-value
PLG	-27.48	0.045*	PLG	-13.63	0.394
ASG	-43.81	0.001*	ASG	-41.10	0.005*
MSG	-16.35	0.034*	MSG	-13.92	0.046*
PSG	-35.62	0.001*	PSG	-12.05	0.404
AIC	-35.10	0.021*	AIC	-11.69	0.450
ALG	-45.36	0.004*	ALG	-34.37	0.040*
ACG	-121.55	0.114	ACG	-237.30	0.002*
Amygdala	-44.06	0.004*	Amygdala	-56.55	<0.0001*
Lat Occ	-82.90	<0.0001*	Lat Occ	-118.05	<0.0001*
Cuneus	-131.80	0.032*	Cuneus	-153.12	0.019*
Lat Orb	-892.50	<0.0001*	Lat Orb	-829.30	<0.0001*
Subgenual	-28.31	0.002*	Subgenual	-38.49	<0.0001*

Table 3.2 Univariate analysis by group to assess difference between surface area of regions of interest in healthy controls and patients with MDD.

Left	Co-efficient	P-value	Right	Co-efficient	P-value
PLG	15.30	0.077	PLG	21.40	0.013*
ASG	-1.44	0.828	ASG	-2.31	0.745
MSG	3.68	0.451	MSG	5.29	0.225
PSG	6.72	0.342	PSG	17.98	0.016*
AIC	50.69	0.004*	AIC	20.18	0.020*
ALG	7.87	0.440	ALG	12.86	0.199
ACG	42.42	0.110	ACG	-5.94	0.829
Amygdala	4.23	0.542	Amygdala	0.23	0.972
Lat Occ	2.95	0.760	Lat Occ	70.39	0.350
Cuneus	77.46	0.030*	Cuneus	67.78	0.055
Lat Orb	45.02	0.571	Lat Orb	-0.775	0.939
Subgenual	1.45	0.769	Subgenual	-5.54	0.293

3.3. Trajectories of Insular Subregions

3.3.1 Volume

As shown in Figures 3.2 and 3.3, the insular subregions across both hemispheres appear to follow similar trajectories exhibiting a decrease in volume over time in both groups. With the exception of the anterior short gyrus and the lateral orbitofrontal cortex, the trajectories of the control and MDD groups for all other subregions shown in the figures appear to intersect in the first half of the lifespan (<30 years of age). The confidence intervals of the control and the MDD groups appear to overlap after this intersection, and for a majority of the subregions (except for the left middle short gyrus, and both left and right anterior long gyri), this overlap ceases after 40 years of age.

These observations are reinforced by the results of the group-age interaction as displayed in Table 3.3. The left PLG, left ALG, left amygdala, left and right ALG, left and right subgenual cortex, right MSG, right ACG, right lateral occipital and right lateral orbitofrontal cortex all showed significance in the group-age interaction for 60-69 and 70-79 years of age. The left AIC was marginally significant for the 60-69 category and the left PSG was marginally significant for the 70-79 category. The left lateral occipital and lateral orbitofrontal, as well as the right cuneus were both significant for the 60-69 category only. The left cuneus was significant for ages 50-69. It is important to note that that a number of control

groups did not fit significantly with any model for age vs. volume that was tested (left MSG, left ALG, and left and right cuneus), suggesting no age associated tissue volume changes.

Figure 3.2 Graphs comparing the trajectories of the control (blue) and MDD (red) groups for regions of interest in the left hemisphere for which significant differences between groups was identified by univariate analysis. The volumes are corrected for relative ICV. Faded blue lines indicate control groups with no significant fits.
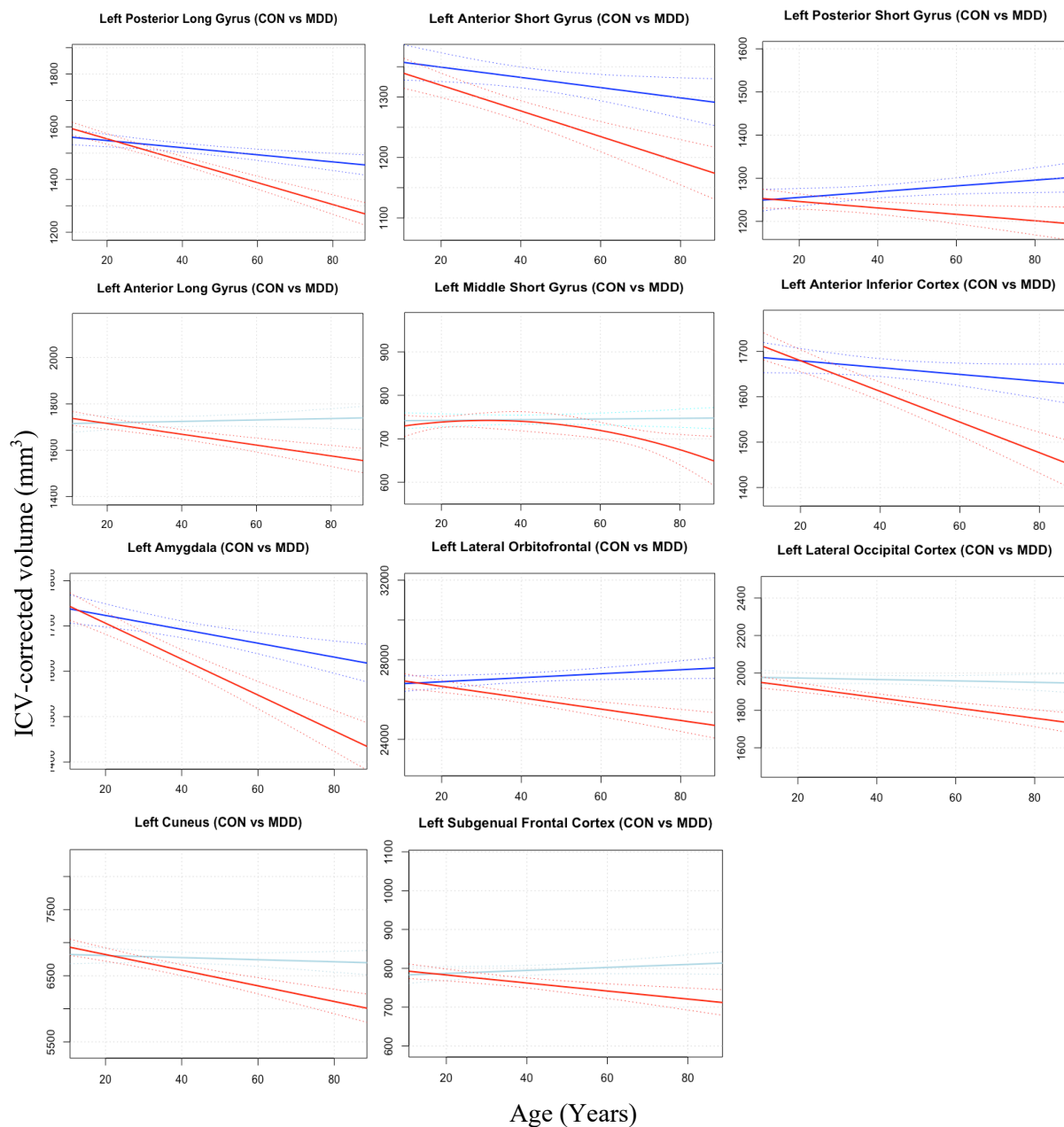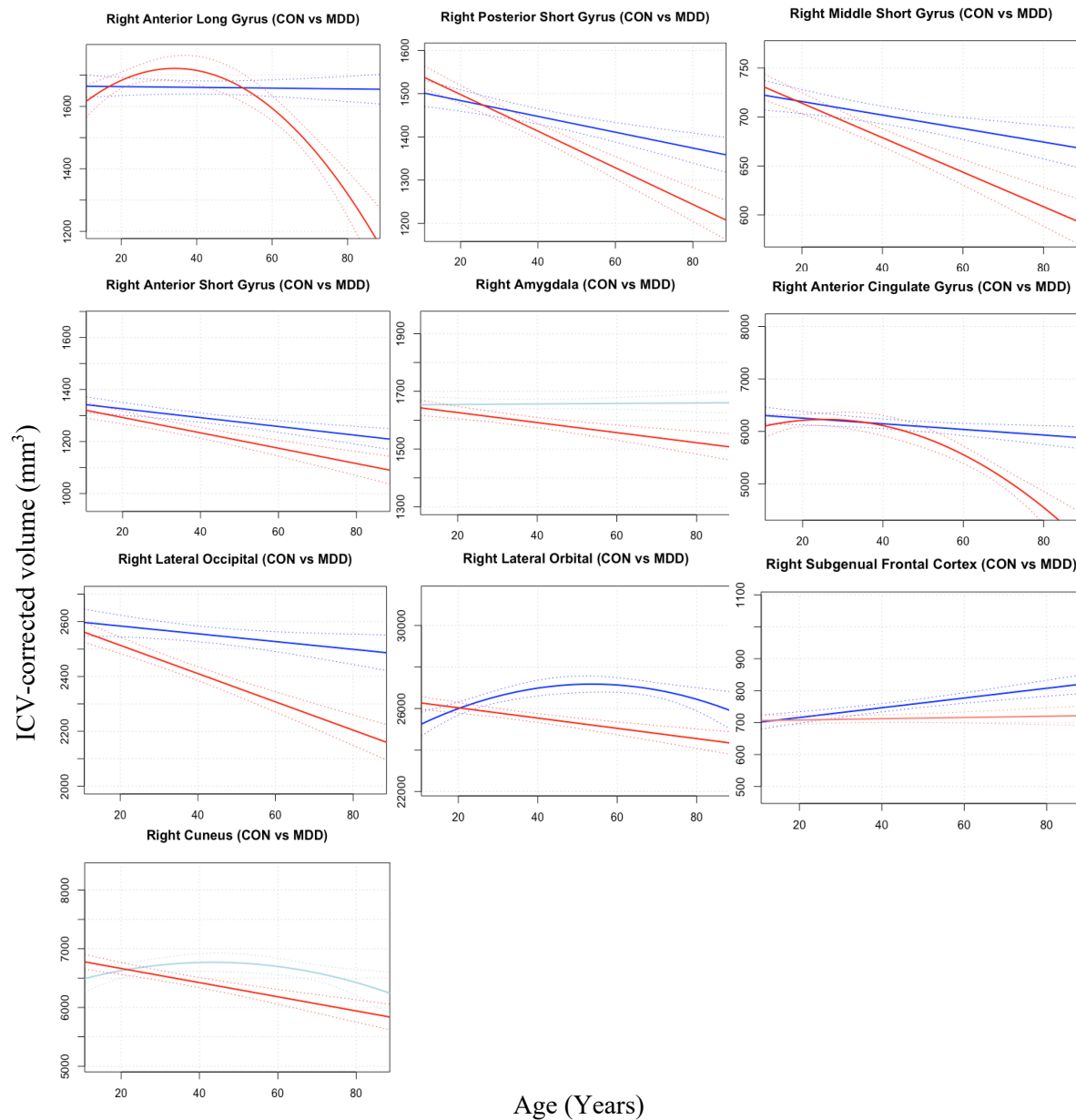
Figure 3.3 Graphs comparing the trajectories of the control (blue) and MDD (red) groups for regions of interest in the right hemisphere for which significant differences between groups was identified by univariate analysis. The volumes are corrected for relative ICV. The faded blue and red lines indicate groups that did not yield significant fits during the modeling stage.

Table 3.3 P-values of group x age interaction for regions with significant group co-efficient in univariate analysis of volume.

ROI	10s	20s	30s	40s	50s	60s	70s	80s
lPLG	0.950	0.780	Ref	0.868	0.305	0.001*	0.003*	0.164
lASG	0.355	0.171	Ref	0.381	0.473	0.435	0.622	0.382
lMSG	0.963	0.880	Ref	0.718	0.495	0.185	0.200	0.166
lPSG	0.971	0.945	Ref	0.429	0.813	0.157	0.073	0.527
lAIC	0.299	0.302	Ref	0.798	0.651	0.059	0.232	0.256
lALG	0.589	0.605	Ref	0.384	0.816	0.021*	0.007*	0.160
lAmy	0.470	0.975	Ref	0.678	0.974	0.0002*	<0.0001*	0.414
lLOcc	0.936	0.807	Ref	0.653	0.965	0.006*	0.173	0.121
lCuneus	0.728	0.480	Ref	0.253	0.003*	0.034*	0.855	0.926
lLOrb	0.147	0.505	Ref	0.880	0.984	0.029*	0.073	0.984
lSub	0.591	0.840	Ref	0.882	0.089	0.003*	0.038*	0.204
rASG	0.417	0.168	Ref	0.132	0.267	0.608	0.827	0.966
rMSG	0.355	0.699	Ref	0.735	0.869	0.011*	0.004*	0.477
rPSG	0.021	0.076	Ref	0.314	0.949	<0.001*	<0.001*	0.188
rALG	0.116	0.588	Ref	0.852	0.578	<0.0001*	<0.0001*	0.069
rACG	0.916	0.958	Ref	0.118	0.604	<0.0001*	<0.0001*	0.084
rAmy	0.299	0.495	Ref	0.756	0.162	0.150	0.634	0.762
rLOcc	0.591	0.565	Ref	0.971	0.833	0.0004*	0.027*	0.198
rCuneus	0.181	0.995	Ref	0.410	0.128	0.0303*	0.240	0.457
rLOrb	0.129	0.648	Ref	0.863	0.646	0.0008*	0.019*	0.762
rSub	0.355	0.913	Ref	0.264	0.214	0.003*	0.025*	0.382

3.3.2 Surface Area

For each of the regions that exhibited a significant difference in surface area between groups in the univariate analysis, the deviations between the two trajectories are subtle (Figure 3.4). Although the analysis showed that the right PLG exhibits a significant difference in surface area-age trajectory, we did not find a significant fit for the control volumes of this region. For the remaining regions (left and right AIC, right PSG and left cuneus), the confidence intervals of each trajectory appear to overlap for a majority of the lifespan with the exception of the sections <10 and >80 years of age. The group-age interaction analysis reveals that of these regions, only the left anterior inferior cortex had a significant interaction between these two variables, for the 10s and the 70s (see Table 3.4).
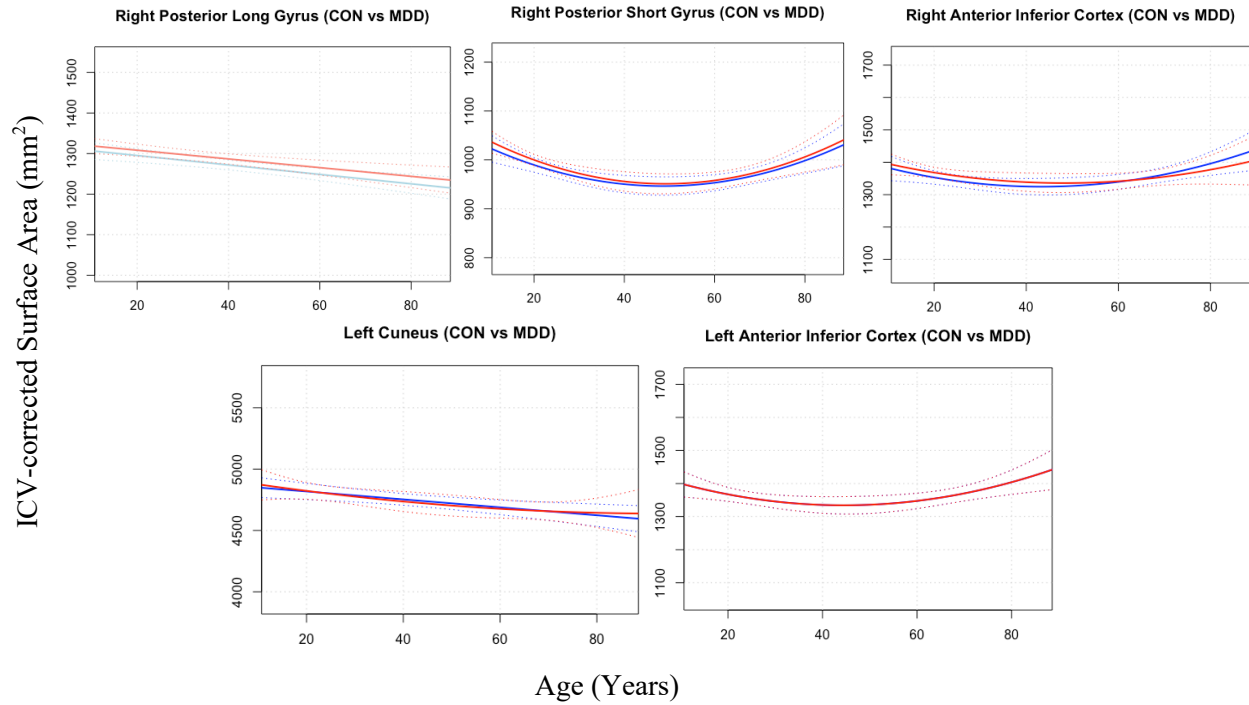
Figure 3.4 Graphs comparing the trajectories of the control (blue) and MDD (red) groups for the insular subregions for which significant differences between groups as identified by univariate analysis. The surface areas are corrected for relative ICV. Faded blue and red lines indicate groups that did not meet significance for any model.

Table 3.4 P-values for group x age interaction for regions with significant group co-efficient in univariate analysis of surface area.

ROI	10s	20s	30s	40s	50s	60s	70s	80s
lAIC	0.034*	0.200	Ref	0.469	0.648	0.106	0.028*	0.456
lCuneus	0.689	0.315	Ref	0.915	0.591	0.188	0.423	0.726
rPLG	0.909	0.388	Ref	0.308	0.299	0.065	0.817	0.794
rPSG	0.150	0.135	Ref	0.595	0.693	0.584	0.050	0.692
rAIC	0.489	0.678	Ref	0.174	0.720	0.400	0.494	0.861

Chapter 4: Discussion

4.1 Implications for neurodevelopment vs. neurodegeneration

The results of the statistical analyses run on our volumetric data, coupled with the visual supplement of the control and MDD trajectories, support the notion of the comorbidity of major depression with neurodegeneration. In the control group, we see a standard decline in volume as reported in other examples of literature, while the MDD trajectories tend to decline at an abnormally faster rate,

especially between the ages of 60-80.[18] A majority of the significant fits for the volumetric data were linear, even though other lifespan studies focused on changes in similar regions often report more complex trajectories (quadratic, cubic, or hybrid). This difference may be attributed to the limited age range of the current study, while other studies tend to include pediatric cases younger than 13 and geriatric cases older than 85.

Furthermore, our results suggest that the trajectories of the MDD group tend to differ by subregion, supporting current literature on the different functionalities of insular subregions. In the right hemisphere, we see a clear division between the anterior and posterior regions of the insula, with the quadratic model of the MDD group in the right ALG (region of the posterior insula) compared to the linear models of the MDD groups in both the right ASG and MSG (regions of the anterior insula). Additionally, the age of intersection and deviation of the trajectories also differ by subregion, providing insight into the a potentially multi-faceted neurodegeneration occurring in patients with MDD within the insula.

For the regions of interest outside of the insula implicated in major depression such as the amygdala, lateral orbitofrontal and the subgenual cortex, we also observed significant differences between the groups. However, while some literature suggests that the cuneus is not implicated in depression, our findings indicate that there was a significant difference between the volumes of the cuneus in healthy controls compared to our MDD patients. As this did not serve as the control region we originally anticipated, it would be worthwhile to run the same analysis on another region to compare the trajectories to regions implicated in depression.

Findings on surface area were not as conclusive as initially hypothesized. Since cortical folding takes place in the earliest stages of development, it is not expected to change over time. The trajectories we visualized in this paper indicate that there could be slight differences in cortical surface area with age, but at least deviations between healthy controls and MDD patients appear to be fairly constant in all regions that exhibited a significant group difference. Additionally, it is important to note that for the few

17

regions (right PSG, left AIC and left cuneus) that exhibited significant group differences in both volume and surface area there could be a potential interactive effect between these two metrics.

4.2 Future steps

In addition to the analyses performed in this study, this dataset also provides an opportunity to assess the cortical thickness and geometric shape of each insular subregion. Obtaining these metrics will require further rigorous analysis of the segmented data and could provide more insight into the neurodevelopmental aspect of major depression.

Future analyses related to this study could focus on the degree to which the parts of the insula that exhibit deviations from normal lifespan trajectories are associated with chronicity of the disease, as well as different psychiatric symptoms of depression. Structural MR fails to capture temporal information about a given region of interest, therefore the current dataset lends itself more to a comparison with the chronicity of the disease rather than the scores of the depression scales used to assess the patients. Chronicity would be represented by the duration of illness, measured from the date of the first depressive episode up to the date of the scan. Additional variables to consider are age of onset of depression and number of depressive episodes.

4.3 Limitations

There are a few limitations of the study design and data in this study. First, segmentation of certain subregions of the insula tends toward overestimation with older age due to contrast changes resulting from white matter demyelination that can lead to boundary ambiguity. In an attempt to avoid this over-segmentation, scans of participants over the age of 85 were excluded from analysis. Another limitation may be the wide variation of volumes per subregion within a given age range, especially within both adolescent cohorts. This variance may be due to the pubertal status of the individual, and additional metrics like BMI could be considered to aid in the division of this cohort into patients who have reached puberty and those who have not. Lastly, the missing MDD cases from the Young Adolescent 2 cohort left

an age gap in the mid-50s to early 60s range, which could slightly affect the significance of the different models fit to the data. Analyses will be rerun once the data are provided.

Chapter 5: Conclusion

The results of this study have furthered our understanding of major depression, particularly in relation to the unique morphometric changes that occur in the subregions of the insula in patients with MDD. Major depression is a complex disorder that requires multiple angles of analysis to fully assess etiology and symptomology. It is important to note that two metrics, volume and surface area, yielded different trajectories within the same subregions. The volumetric data showed a clear co-morbidity with age, while surface area data was largely inconclusive with regards to neurodevelopment and neurodegeneration.

With an ever-growing need for biomarkers of psychiatric illnesses, the findings of this project could contribute to a better understanding of the etiology of major depression and support precision medicine's goal of providing personalized care for every individual. Currently, most patients suffering from MDD are treated with the same medications or behavioral therapy, often regardless of age. Results from analyses like those run in this study could help tailor a patient's treatment plan by providing information about the point and duration of deviation of specific subregions of the insula, a brain region well-implicated in psychiatric illnesses including major depression.

References:

1) World Health Organization. (2018, March 22). *Depression. Retrieved from*

   https://www.who.int/news-room/fact-sheets/detail/depression

2) Craig, A. D. (2002). How do you feel? Interoception: the sense of the physiological condition of

   the body. *Nature reviews neuroscience*, *3*(8), 655.

3) Uddin, L. Q., Nomi, J. S., Hébert-Seropian, B., Ghaziri, J., & Boucher, O. (2017). Structure and

   function of the human insula. *Journal of clinical neurophysiology: official publication of the*

   American Electroencephalographic Society, *34*(4), 300.

4) Wise, T., Radua, J., Via, E., Cardoner, N., Abe, O., Adams, T. M., ... & Dickstein, D. P. (2017).

   Common and distinct patterns of grey-matter volume alteration in major depression and bipolar

   disorder: evidence from voxel-based meta-analysis. *Molecular psychiatry*, *22*(10), 1455.

5) Peng, W., Chen, Z., Yin, L., Jia, Z., & Gong, Q. (2016). Essential brain structural alterations in

   major depressive disorder: a voxel-wise meta-analysis on first episode, medication-naive patients.

   Journal of affective disorders, *199*, 114-123.

6) Faillenot, I., Heckemann, R. A., Frot, M., & Hammers, A. (2017). Macroanatomy and 3D

   probabilistic atlas of the human insula. *NeuroImage*, *150*, 88-98.

7) Ghaziri, J., Tucholka, A., Girard, G., Boucher, O., Houde, J. C., Descoteaux, M., ... & Nguyen, D.

   K. (2018). Subcortical structural connectivity of insular subregions. *Scientific reports*, *8*(1), 8596.

8) Afif, A., Bouvier, R., Buenerd, A., Trouillas, J., & Mertens, P. (2007). Development of the

   human fetal insular cortex: study of the gyration from 13 to 28 gestational weeks. *Brain Structure*

   and Function, *212*(3-4), 335-346.

9) Rana, S., Shishegar, R., Quezada, S., Johnston, L., Walker, D. W., & Tolcos, M. (2019). The

   Subplate: A Potential Driver of Cortical Folding?. *Cerebral Cortex*.

10) Shaw, P., Kabani, N. J., Lerch, J. P., Eckstrand, K., Lenroot, R., Gogtay, N., ... & Giedd, J. N. (2008). Neurodevelopmental trajectories of the human cerebral cortex. *Journal of Neuroscience*, *28*(14), 3586-3594.

11) Avants, B. B. et al. A reproducible evaluation of ANTs similarity metric performance in brain image registration. Neuroimage 54, 2033–2044 (2011).

12) Johnson, W. E., Li, C., & Rabinovic, A. (2007). Adjusting batch effects in microarray expression data using empirical Bayes methods. *Biostatistics*, *8*(1), 118-127.

13) Fortin, J. P., Parker, D., Tunç, B., Watanabe, T., Elliott, M. A., Ruparel, K., ... & Schultz, R. T. (2017). Harmonization of multi-site diffusion tensor imaging data. *Neuroimage*, *161*, 149-170.

14) Fortin, J. P., Cullen, N., Sheline, Y. I., Taylor, W. D., Aselcioglu, I., Cook, P. A., ... & McInnis, M. (2018). Harmonization of cortical thickness measurements across scanners and sites. *NeuroImage*, *167*, 104-120.

15) Coupé, P., Catheline, G., Lanuza, E., Manjón, J. V., & Alzheimer's Disease Neuroimaging Initiative. (2017). Towards a unified analysis of brain maturation and aging across the entire lifespan: A MRI analysis. *Human brain mapping*, *38*(11), 5501-5518.

16) Coupé, P., Manjón, J. V., Lanuza, E., & Catheline, G. (2019). Lifespan Changes of the Human Brain In Alzheimer's Disease. *Scientific reports*, *9*(1), 3998.

17) R Core Team (2014). R: A language and environment for statistical computing. R Foundation for Statistical Computing, Vienna, Austria. URL http://www.R-project.org/

18) Ge, Y., Grossman, R. I., Babb, J. S., Rabin, M. L., Mannon, L. J., & Kolson, D. L. (2002). Age-related total gray matter and white matter changes in normal adult brain. Part I: volumetric MR imaging analysis. *American journal of neuroradiology*, *23*(8), 1327-1333.

Appendix I:

Univariate analysis of age as a categorical variable with the 30s as a reference group for the volumetric data for both hemispheres.

Left	10s	20	30	40	50	60	70	80
PLG	<0.0001*	0.032*	Ref	0.062	0.133	0.006*	0.005*	0.333
ASG	0.121	0.465	Ref	0.429	0.327	0.110	0.043*	0.636
MSG	0.619	0.578	Ref	0.171	0.015*	0.861	0.279	0.987
PSG	0.172	0.940	Ref	0.656	0.072	0.152	0.552	0.275
AIC	0.0003*	0.027*	Ref	0.135	0.380	0.934	0.320	0.422
ALG	0.037*	0.399	Ref	0.458	0.076	0.636	0.763	0.817
ACG	0.917	0.958	Ref	0.118	0.604	<0.0001*	<0.0001*	0.084
Amyg	0.470	0.975	Ref	0.678	0.974	<0.001*	<0.0001*	0.414
L Occ	0.020*	0.252	Ref	0.113	0.158	0.795	0.408	0.887
Cuneus	0.013*	0.157	Ref	0.339	0.008*	0.878	0.128	0.109
L Orb	0.881	0.551	Ref	0.837	0.035*	0.834	0.236	0.427
Sub	0.921	0.868	Ref	0.835	0.482	0.613	0.141	0.625

Right	10s	20	30	40	50	60	70	80
PLG	0.960	0.689	Ref	0.395	0.553	<0.0001*	<0.0001*	0.002*
ASG	0.222	0.179	Ref	0.005*	0.450	0.007*	<0.0001*	0.323
MSG	0.006*	0.050*	Ref	0.271	0.223	0.019*	0.003*	0.462
PSG	0.0004*	0.063	Ref	0.878	0.476	0.001*	0.0003*	0.245
AIC	0.033*	0.064	Ref	0.108	0.772	0.0004*	<0.0001*	0.025*
ALG	0.790	0.641	Ref	0.267	0.098	0.010*	0.002*	0.368
ACG	0.670	0.512	Ref	0.577	0.399	<0.0001*	<0.0001*	0.069
Amyg	0.299	0.495	Ref	0.756	0.162	0.634	0.150	0.762
L Occ	0.332	0.989	Ref	0.444	0.582	0.002*	<0.0001*	0.009*
Cuneus	0.250	0.384	Ref	0.406	0.166	0.256	0.048*	0.297
L Orb	0.034*	0.279	Ref	0.662	0.037*	0.243	0.024*	0.205
Sub	0.691	0.831	Ref	0.299	0.043*	0.009*	0.031*	0.003*

Appendix II:

Univariate analysis of sex (male) for the volumetric data for both hemispheres.

Left ROI	Co-efficient	P-value
PLG	-33.026	0.018*
ASG	-23.593	0.069
MSG	-8.940	0.256
PSG	-26.380	0.016*
ALG	-51.968	0.0007*
AIC	-31.090	0.052
ACG	9.245	0.906
Amygdala	42.255	0.007*
Lateral occipital	-18.76	0.259
Cuneus	6.904	0.912
Lateral orbitofrontal	-571.3	0.002*
Subgenual	12.493	0.190

Right ROI	Co-efficient	P-value
PLG	-28.440	0.080
ASG	4.421	0.769
MSG	-0.170	0.981
PSG	-10.087	0.492
ALG	-33.219	0.034*
AIC	-28.270	0.097
ACG	1.528	0.984
Amygdala	35.889	0.005*
Lateral occipital	0.859	0.969
Cuneus	43.77	0.509
Lateral orbitofrontal	-545.9	0.001*
Subgenual	0.375	0.969

Appendix III:

Univariate analysis of age as a categorical variable with the 30s as a reference group for the surface area data for both hemispheres.

Left	10s	20	30	40	50	60	70	80
PLG	<0.0001*	0.104	Ref	0.185	0.128	0.016*	0.091	0.543
ASG	0.002*	0.728	Ref	0.369	0.157	0.015*	0.077	0.172
MSG	0.003*	0.432	Ref	0.134	0.049*	0.007*	0.042*	0.252
PSG	0.0002*	0.666	Ref	0.680	0.114	<0.0001*	0.0002*	0.052
AIC	<0.0001*	0.002*	Ref	0.108	0.140	<0.0001*	<0.0001*	0.063
ALG	0.001*	0.488	Ref	0.480	0.090	<0.0001*	0.001*	0.168
ACG	0.056	0.927	Ref	0.368	0.357	0.165	0.186	0.486
Amyg	<0.0001*	0.721	Ref	0.718	0.392	0.008*	0.059	0.052
L Occ	<0.0001*	0.101	Ref	0.241	0.373	0.033*	0.034*	0.275
Cuneus	<0.0001*	0.126	Ref	0.223	0.021	0.052	0.557	0.435
L Orb	0.0002*	0.196	Ref	0.484	0.035*	0.001*	0.010*	0.504
Sub	0.011*	0.485	Ref	0.373	0.255	0.004*	0.139	0.394

Right	10s	20	30	40	50	60	70	80
PLG	0.047*	0.685	Ref	0.319	0.468	0.584	0.641	0.291
ASG	0.015*	0.369	Ref	0.036*	0.375	0.110	0.495	0.294
MSG	<0.0001*	0.089	Ref	0.255	0.203	0.020*	0.115	0.483
PSG	<0.0001*	0.090	Ref	0.921	0.283	0.017*	0.068	0.368
AIC	<0.0001*	0.156	Ref	0.110	0.936	0.047*	0.163	0.750
ALG	0.005*	0.683	Ref	0.428	0.110	0.012*	0.071	0.461
ACG	0.198	0.399	Ref	0.642	0.138	0.517	0.965	0.851
Amyg	0.001*	0.363	Ref	0.761	0.109	<0.0001*	<0.0001*	0.037*
L Occ	0.114	0.526	Ref	0.964	0.060	0.056	0.367	0.801
Cuneus	<0.0001*	0.262	Ref	0.441	0.116	0.168	0.675	0.869
L Orb	0.015*	0.417	Ref	0.249	0.454	0.298	0.116	0.055
Sub	0.044*	0.674	Ref	0.141	0.021*	<0.0001*	<0.0001*	0.008*

Appendix IV:

Univariate analysis of sex for the surface area data for both hemispheres.

Left ROI	Co-efficient	P-value
PLG	-62.14	<0.0001*
ASG	-46.02	<0.001*
MSG	-29.58	<0.0001*
PSG	-47.75	<0.0001*
ALG	-72.90	<0.0001*
AIC	-64.10	<0.0001*
ACG	-148.68	<0.0001*
Amygdala	-27.86	<0.001*
Lateral occipital	-69.26	<0.0001*
Cuneus	-174.50	<0.0001*
Lateral orbitofrontal	-603.41	<0.0001*
Subgenual	-21.18	<0.001*
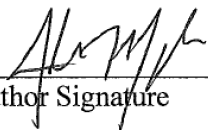
Right ROI	Co-efficient	P-value
PLG	-60.85	<0.0001*
ASG	-31.58	<0.0001*
MSG	-24.64	<0.0001*
PSG	-48.58	<0.0001*
ALG	-63.02	<0.0001*
AIC	-70.93	<0.0001*
ACG	-153.83	<0.0001*
Amygdala	-229.29	<0.0001*
Lateral occipital	-606.57	<0.0001*
Cuneus	-156.41	<0.0001*
Lateral orbitofrontal	-66.83	<0.0001*
Subgenual	-23.83	<0.0001*

Publishing Agreement

It is the policy of the University to encourage the distribution of all theses, dissertations, and manuscripts. Copies of all UCSF theses, dissertations, and manuscripts will be routed to the library via the Graduate Division. The library will make all theses, dissertations, and manuscripts accessible to the public and will preserve these to the best of their abilities, in perpetuity.

Please sign the following statement:

I hereby grant permission to the Graduate Division of the University of California, San Francisco to release copies of my thesis, dissertation, or manuscript to the Campus Library to provide access and preservation, in whole or in part, in perpetuity.

_____
Author Signature

_____9 . 10 . 19_____
Date